JOURNAL OF PROPULSION AND POWER
Vol. 23, No. 4, July–August 2007

Development of Scalable Space–Time Averaged Regression Rate Expressions for Hybrid Rockets

M. Arif Karabeyoglu* and Brian J. Cantwell†
Stanford University, Stanford, California 94306
and
Greg Zilliac‡
NASA Ames Research Center, Mountain View, California 94085

DOI: 10.2514/1.19226

The fuel regression rate expressions reported in the hybrid literature often depend explicitly on the physical dimensions of the system such as the fuel port diameter. Typically, when these dimensional formulas are applied to systems with significantly different scales, they produce grossly inaccurate results. This paper addresses the development of scalable space–time averaged regression rate formulas for hybrid rockets. The derivation process hinges on the assumption that the local instantaneous regression rate is a function of the local mass flux and the axial port distance in the power law format as predicted by the classical theory developed by Marxman. In this study, we have developed physics-based nondimensional formulas for the space–time averaged regression rate and used these expressions to develop a scalable regression rate law for a selected propellant combination, paraffin-based SP-1a/GOX, from limited motor data. Initially, space and time averaging are treated separately, which were later combined to develop a technique that allows for the coupling between the spatial and time variations to predict the port diameter and mass flow rate profiles as functions of time. Finally, a comprehensive technique to estimate the systematic and random errors on the regression rate and mass flux data is also outlined.

Nomenclature

A_{port}	=	local port area
A_{or}	=	orifice area
a	=	regression rate coefficient
B_G	=	mass flow equation parameter
C_D	=	diameter equation coefficient
Cd	=	discharge coefficient of the orifice
C_m	=	mass flux equation coefficient
C_{port}	=	local port circumference
c_o^*	=	characteristic velocity of the oxidizer
D	=	hydraulic diameter of the port
E	=	relative error
Error	=	error relative to the exact mass flux
f_o	=	O/F function for the oxidizer flux case
f_t	=	O/F function for the total flux case
G	=	local mass flux in the port
$\bar{G}_{\text{oA}}$	=	area averaged oxidizer mass flux
$\bar{G}_{\text{oD}}$	=	diameter averaged oxidizer mass flux
$\bar{G}_{\text{oE}}$	=	exact oxidizer mass flux
$\bar{G}_{\text{oF}}$	=	flux averaged oxidizer mass flux
G_o	=	oxidizer mass flux
G_t	=	total mass flux
L	=	grain length
m	=	length exponent
$\dot{m}$	=	local mass flow rate in the port
$\dot{m}_o$	=	oxidizer mass flow rate
$\dot{m}_t$	=	total mass flow rate
n	=	mass flux exponent
O/F	=	oxidizer to fuel ratio of the motor
P_f	=	orifice upstream pressure
R	=	final to initial port diameter ratio, D_f/D_i
$\dot{r}$	=	regression rate
$\dot{r}_L$	=	regression rate at the exit plane
$\dot{r}_{\text{min}}$	=	minimum regression rate
$\dot{r}_{\text{raw}}$	=	regression rate before O/F correction
t_b	=	burn time
$V_{\text{port}x}$	=	volume of the port from the leading edge to an arbitrary point x
x	=	axial distance
x_{min}	=	distance at minimum regression rate
α	=	O/F parameter, oxidizer flux case
β	=	O/F parameter, total flux case
ΔM_f	=	total mass of the fuel burned
κ	=	mass flux coefficient
ρ_f	=	fuel density

Subscripts

f	=	final
i	=	initial

Superscripts

-	=	averaged quantity
$\sim$	=	dummy variable

Presented as Paper 3544 at the AIAA/ASMA/ASEE Joint Propulsion Conference, Tucson, AZ, 10–13 July 2005; received 21 September 2005; revision received 1 August 2006; accepted for publication 18 August 2006.

*President and Chief Technical Officer, Space Propulsion Group, Inc., Consulting Professor, Stanford University.
†Chairman, Edward C. Wells Professor, Department of Aeronautics and Astronautics, Stanford University.
‡Research Scientist, NASA Ames Research Center.

I. Introduction

AS DISCUSSED extensively in the literature, hybrid rockets offer many advantages over conventional liquid and solid systems. One of the most important advantages is the hybrid's inherent safety, which is a direct consequence of the storage of the fuel and oxidizer remotely from each other in different phases (one in liquid, the other in solid, making it virtually impossible for them to mix and react spontaneously). The two-phase propellant system also forces hybrids to operate in a heterogeneous, boundary layer, combustion configuration. Typically, the hybrid combustion process

is diffusion limited, making the fuel regression rate primarily mass flux dependent. In practice, the accurate ballistic design of a hybrid system requires the full understanding of the dependence of the regression rate on the mass flux and other key operational parameters such as pressure and grain length. This functional relation is commonly referred to as the "regression rate law" and each propellant combination has its unique regression rate formula due to the differences in the thermophysical and thermochemical properties of the components of the propellant. Because of the lack of fidelity in the combustion models presently available for hybrid rockets, an accurate theoretical determination of the regression rate law based on the fundamental properties of the propellants is still not possible. Even though there are theories that can predict the form of the regression rate dependency on system properties, none of these prediction tools can accurately estimate the regression rate behavior of a system in a manner that is required in the internal ballistic design process.

Consequently, in practice, the regression rate law for each hybrid propellant system of interest must be constructed from extensive motor testing. The interpretation of the motor data and the reduction to a scalable regression rate law is a difficult process. The methods of data reduction are not unique due to the nonlinear nature of the problem and, for certain test conditions, each method may yield significantly different results. In many reports and papers, the technique used in the data reduction process is not adequately discussed, decreasing the value of the information. In certain cases, the regression rate is written in terms of dimensional parameters other than the oxidizer or total mass flux, resulting in formulas that are accurate for interpolation purposes but potentially highly problematic when they are used to extrapolate to other scales. One example to such a scaling formula is given in [1], which assumes a regression rate law that shows an explicit and strong dependency on the average port diameter.

$$\bar{\dot{r}} = 0.065\bar{G}_o^{0.77}\left[\frac{\bar{D}}{3}\right]^{0.71}$$

When this formula is used to predict the regression rate of a system 10 times larger in scale, one estimates a regression rate approximately five times higher. Clearly, such an increase in regression rate with motor scale is highly unrealistic.

Our goal in this study is to develop space–time averaged regression rate expressions from the classical local instantaneous regression rate equation in the power law format. The mass flux and axial distance exponents will be kept as free parameters to preserve the generality in the derived formulas.

In the first part of the paper, we concentrate on developing a space-averaged regression rate law with a nondimensional correction term. Two laws will be given: one based on the oxidizer mass flux and the other on the total mass flux. It will be shown that the correction formulas, which are functions of O/F alone, show that both the oxidizer flux and total flux based regression rate laws produce similar levels of error (the formula based on the total flux being slightly more accurate). Later in the section, the scaling formulas are applied to paraffin-based motor test data to successfully reduce the scatter in the regression rate–mass flux plane.

In the second part, we discuss the issues associated with time averaging. This is an important consideration for estimating a regression rate law from motor test data because, unlike the regression rate, the mass flux is a nonlinear quantity (ratio of the mass flow rate to the port area). This nonlinear character permits several means of time averaging for the mass flux. The commonly used ones are based on the average port diameter, average port area, and average mass flux. It is important to note that all of these methods are approximations and they would produce different regression rate laws for a given set of motor test data. As it is shown in the following sections, the most accurate method is based on the average port diameter.

A section on the error analysis including the effects of the random measurement and systematic errors is also included. The issues associated with the selection process of the optimum burn time (i.e., for minimum combined error) for the regression rate evaluation tests are discussed.

In the final part of this paper, the coupling of space and time averaging processes will be examined. The partial differential equations that govern the regression rate in the fuel port as a function of time and axial distance will be constructed. Some numerical simulations will be conducted to gain insight into the issue of space–time coupled regression rate of the fuel grain. Some paraffin motor tests will be used as examples to understand the axial variation of the regression rate.

II. Scaling Law for the Local Instantaneous Regression Rate

A universally acceptable and highly accurate theory to predict the local regression rate of a hybrid fuel grain, at a given instant of the motor operation, does not exist. Most complete models developed to date are the classical diffusion limited theory by Marxman et al. [2] and semi-empirical relations developed by Chiaverini et al. [3]. For the sake of simplicity, we will take the classical theory as the baseline in our derivations. Similar results can also be obtained by using Chiaverini's more extensive regression rate scaling relations.

According to the diffusion limited theory developed by Marxman et al. [2], the local instantaneous recession velocity of the hybrid fuel can be expressed as a power law formula in terms of the local mass flux and the axial position in the port.

$$\dot{r} = aG^n x^m \tag{1}$$

The classical values for the mass flux and length exponents are 0.8 and −0.2, respectively. These values originate from turbulent boundary layer heat transfer arguments and were derived for a fully turbulent boundary layer developing over a flat plate with no dilution of the oxidizer in the freestream along the axis of the cylindrical port. In reality, the combustion process that takes place in a hybrid rocket is much more complex. First of all, the diffusion flame that forms over the surface conforms to the cylindrical internal geometry of the fuel port. Consequently, downstream of the axial location that the boundary layers merge, the oxidizer concentration along the centerline starts to decrease due to the dilution induced by the combustion products. This fact, along with many other complicating factors that are not included in the relatively simple model, such as the variation of the blowing parameter with length, result in mass flux and length exponents that are significantly different from the values predicted by the diffusion limited theory. In fact, the flux exponent is reported to be in the range of 0.5–0.8 for most hybrid systems.

The coefficient a can be assumed to be constant for a given combination of propellants. We like to note that under extreme mass flux conditions (i.e., very high or very low) or for metal loaded fuel systems, the regression rate expression becomes pressure dependent. In this case, the coefficient a can be taken as a function of the chamber pressure. For the operating conditions encountered in typical hybrid rocket applications the effect of pressure on the regression rate is generally negligible and for the sake of simplicity it will be ignored in this paper. We would like to note that the results of the following sections can easily be extended to a system with pressure dependent operation.

III. Space Averaging

In this section, we concentrate on averaging of the regression rate over the burning surface of the fuel grain. For the sake of simplicity, the regression rate is assumed to be constant around the circumference of the fuel port at any given axial location. Note that this is a fairly good approximation for circular ports, but loses its validity for port shapes with sharp corners. Note that the introduction of this assumption simplifies the two-dimensional space-averaging problem down to the one-dimensional length averaging of the regression rate.

We start with the mass balance in the fuel port, which can be expressed as

$$\frac{d\dot{m}}{dx} = \rho_f C_{\text{port}} \dot{r} \tag{2}$$

Following the substitution of the local instantaneous regression rate expression given by Eq. (1), the mass balance expression reduces to a first-order nonlinear ordinary differential equation for the local mass flow rate

$$\frac{d\dot{m}}{dx} = B_G \dot{m}^n x^m \tag{3}$$

Here, we have used the definition of the mass flux $G \equiv \dot{m}/A_{\text{port}}$ and introduced the following parameter for convenience

$$B_G = a\rho_f \frac{C_{\text{port}}}{A_{\text{port}}^n} \tag{4}$$

Note that B_G follows the scaling law

$$B_G \propto \frac{C_{\text{port}}}{A_{\text{port}}^n} \propto D^{1-2n} \tag{5}$$

In general, both the circumference and the port area are functions of the port hydraulic diameter which is expected to vary with axial distance. For most hybrid rocket systems the flux exponent is in the range of 0.5–0.7 and, consequently, the hydraulic diameter dependency of B_G is quite weak. Furthermore, for typical hybrid applications, the change in the port area with axial distance is also small, typically less than 10% (see [3]). For that reason, B_G will be assumed to be constant and its value will be evaluated using the space-averaged hydraulic diameter of the port. Following this approximation, Eq. (3) can easily be integrated by separation of variables.

A. Oxidizer Flux Scaling

Our goal in this section is to derive an expression for the regression rate in terms of the oxidizer mass flux. We start by integrating Eq. (3), which yields the following mass flow rate distribution in the port.

$$\frac{\dot{m}}{\dot{m}_o} = \left[1 + \alpha\left(\frac{x}{L}\right)^{(m+1)}\right]^{1/(1-n)} \tag{6}$$

where

$$\alpha = \frac{1-n}{1+m} B_G \frac{L^{m+1}}{\dot{m}_o^{1-n}} \tag{7}$$

Upon the substitution of Eq. (6) in Eq. (1), the local instantaneous regression rate can be written explicitly as

$$\dot{r} = \frac{a\dot{m}_o^n L^m}{A_{\text{port}}^n}\left[1 + \alpha\left(\frac{x}{L}\right)^{(m+1)}\right]^{n/(1-n)}\left(\frac{x}{L}\right)^m \tag{8a}$$

Here, we will neglect the axial variation of port area and introduce the oxidizer mass flux as $G_o \equiv \dot{m}_o/A_{\text{port}}$, where A_{port} is calculated using the space-averaged diameter. Again, this assumption can be justified for hybrids because the axial variation of the port diameter is small. Note that in Sec. VI of this paper, the constant port area approximation will be eliminated. Using the definition of the oxidizer mass flux, Eq. (8a) can be expressed as

$$\dot{r} = aG_o^n L^m [1 + \alpha(x/L)^{(m+1)}]^{n/(1-n)}(x/L)^m \tag{8b}$$

We define the space-average regression rate as follows.

$$\bar{\dot{r}} = \int_0^1 \dot{r}(x/L)\, \mathrm{d}(x/L) \tag{9}$$

Equation (9), following the substitution of the local regression rate given by Eq. (8), can be integrated by parts to yield the following closed form solution for the average regression rate.

$$\bar{\dot{r}} = \frac{aG_o^n L^m (1-n)}{\alpha(1+m)}[(1+\alpha)^{1/(1-n)} - 1] \tag{10}$$

Independently, average regression rate and oxidizer to fuel ratio of the motor are related according to the following formula

$$\frac{\bar{\dot{r}}}{aG_o^n L^m} = \frac{1}{O/F}\frac{1}{B_G}\frac{\dot{m}_o^{1-n}}{L^{1+m}} \tag{11}$$

where the oxidizer to fuel ratio is defined as

$$O/F = \frac{\dot{m}_o}{\rho_f L C_{\text{port}} \bar{\dot{r}}} \tag{12}$$

Using the definition of α, one can write the relation

$$\frac{\bar{\dot{r}}}{aG_o^n L^m} = \frac{1}{O/F}\frac{1-n}{1+m}\frac{1}{\alpha} \tag{13}$$

After combining Eqs. (10) and (13), one obtains the following formula for α in terms of O/F and n.

$$\alpha = \left(1 + \frac{1}{O/F}\right)^{1-n} - 1 \tag{14}$$

Upon substitution of this expression for α in Eq. (13), one finds an exact formula for the space-averaged regression rate in terms of the motor O/F, n, and m.

$$\frac{\bar{\dot{r}}}{aG_o^n L^m} = \frac{1}{1+m}\frac{1-n}{\{[1+1/(O/F)]^{1-n} - 1\}O/F} = f_o(O/F) \tag{15}$$

It is key to note that the only operational variable that appears in the correction term is the motor O/F.

B. Total Mass Flux Scaling

Similarly, the regression rate law in terms of the total flux can be derived as follows. The ordinary differential equation for the mass flow rate, Eq. (3), can be integrated from an arbitrary axial point x to the end of the fuel grain to obtain the following mass flow rate distribution in the port.

$$\frac{\dot{m}}{\dot{m}_t} = \left\{1 - \beta\left[1 - \left(\frac{x}{L}\right)^{(m+1)}\right]\right\}^{1/(1-n)} \tag{16a}$$

Note that β is defined as

$$\beta = \frac{1-n}{1+m} B_G \frac{L^{m+1}}{\dot{m}_t^{1-n}} \tag{16b}$$

This formula is similar to Eq. (6) but written in terms of the total mass flow rate instead of oxidizer mass flow rate as in Eq. (6).

Upon the substitution of Eq. (16a) in Eq. (1), the local instantaneous regression rate can be written explicitly as

$$\dot{r}(x) = aG_t^n L^m \{1 - \beta[1 - (x/L)^{(m+1)}]\}^{n/(1-n)}(x/L)^m \tag{17}$$

After inserting this formula in the average regression rate expression, Eq. (9), and integrating by parts, one obtains the following closed form solution.

$$\bar{\dot{r}} = \frac{aG_t^n L^m (1-n)}{(1+m)}\frac{[1-(1-\beta)^{1/(1-n)}]}{\beta} \tag{18}$$

Independently, a formula relating the average regression rate to motor O/F can be written as

$$\frac{\bar{\dot{r}}}{aG_t^n L^m} = \frac{1}{(O/F+1)}\frac{1}{B_G}\frac{\dot{m}_t^{1-n}}{L^{1+m}} \tag{19}$$

where the oxidizer to fuel ratio is

$$O/F = \frac{\dot{m}_t}{\rho_f L C_{\text{port}} \bar{\dot{r}}} - 1 \tag{20}$$

Using the definition of β, the following formula can be derived.

$$\frac{\bar{\dot{r}}}{aG_t^n L^m} = \frac{1}{(O/F+1)} \frac{1-n}{1+m} \frac{1}{\beta} \tag{21}$$

After combining Eqs. (18) and (21), one obtains the following expression for β.

$$\beta = 1 - \left(\frac{O/F}{O/F+1}\right)^{1-n} \tag{22}$$

Finally, upon the substitution of Eq. (22) for β in Eq. (18), the exact formula for the space-averaged regression rate can be written as

$$\frac{\bar{\dot{r}}}{aG_t^n L^m} = \frac{1}{1+m} \frac{1-n}{\{1-[(O/F)/(1+O/F)]^{1-n}\}(1+O/F)} = f_t(O/F) \tag{23}$$

C. Regression Rate Variation

It is important to understand the variation of the regression rate with the axial distance which can be achieved by studying the local regression rate formula, Eq. (8b). Because it is convenient to work with nondimensional variables, Eqs. (8b) and (10) have been combined to derive an expression for the nondimensional regression rate (normalized with respect to the average value).

$$\frac{\dot{r}}{\bar{\dot{r}}} = \frac{1+m}{1-n} O/F\alpha[1+\alpha(x/L)^{(m+1)}]^{n/(1-n)}(x/L)^m \tag{24}$$

We would like to remind that α is a function of O/F and is given by Eq. (14). At the exit plane, $x = L$, the nondimensional regression rate reduces to the following form.

$$\frac{\dot{r}_L}{\bar{\dot{r}}} = \frac{1+m}{1-n} O/F\alpha(1+\alpha)^{n/1-n} \tag{25}$$

The form of Eq. (24) suggests that the regression rate takes a minimum value due to the balance between the flux term and the length effect. The value and the position of the minimum regression rate can easily be determined by using the following relationships.

$$\frac{\dot{r}_{\min}}{\dot{r}_L} = \left[\frac{(2n-1)m+1}{(1+\alpha)(mn+1)}\right]^{n/1-n} \left[\frac{m(n-1)}{\alpha(mn+1)}\right]^{m/m+1} \tag{26a}$$

$$\frac{x_{\min}}{L} = \left[\frac{-m(1-n)}{\alpha(mn+1)}\right]^{1/m+1} \tag{26b}$$

Note that the minimum regression rate is normalized with respect to the maximum value which is expected to take place at the exit plane. Also note that for $m \geq 0$, the minimum ceases to exist at an interior point and the lowest value of the regression rate takes place at the entrance plane, $x = 0$.

D. Discussion of the Results for Space Averaging

It is important to start the discussions by stating that the scaling formulas for the space-averaged regression rate given by Eqs. (15) and (23) are in the nondimensional format. The left-hand side of the equation (in either case) is an average regression rate normalized by the local formula [i.e., Eq. (1)], evaluated using either the oxidizer or the total mass flux depending on the case of interest. The right-hand side is a correction for the space averaging in terms of the nondimensional parameters of flux and length exponents and the O/F of the motor. It is instructive to separate the nondimensional correction into two parts:

1) Length effect is given by $1/(1+m)$, which originates from the integration of the direct effect of axial distance (i.e., x^m) in the local regression rate expression. The primary physical cause of this term is the boundary-layer thickening.

2) Flux effect is represented by the complex functions of O/F, $f_o/(1+m)$, and $f_t/(1+m)$. This term is induced by the continuous fuel mass addition in the port.

Please note that the exact form of the correction for the oxidizer and total mass flux formulas are different, as expected. Let us first consider the limiting case, as the O/F goes to infinity. In this case, which corresponds to a very short motor or very slow burning fuel, the O/F correction functions converge to unity and consequently the flux averaging part of the correction disappears.

In Fig. 1, correction functions for both the oxidizer flux formula and total flux formula are plotted as a function of O/F for various n exponents [i.e., Eqs. (15) and (23)]. As indicated by the figure, both corrections are more critical at lower O/F ratios for which the relative increase in the flux along the port length is more pronounced. Figure 1 also reveals that the correction grows with increasing flux exponent n. In the limiting case of $n = 0$, the functions become unity as the regression rate becomes insensitive to the local mass flux. We would like to note that this case has no practical importance in hybrid rockets, because the regression rate presents a strong dependence on the mass flux.

The absolute values of the corrections are plotted in Fig. 2 for the case of $n = 0.62$. The important observation from this figure (and also from Fig. 1 for other n values) is that the total mass flux method produces slightly more accurate results if not corrected for the space averaging. This observation is consistent with the general perception in the hybrid field to express the regression rate law in terms of the total flux for better accuracy. The difference between the two approaches becomes less pronounced at higher O/F values. In fact,

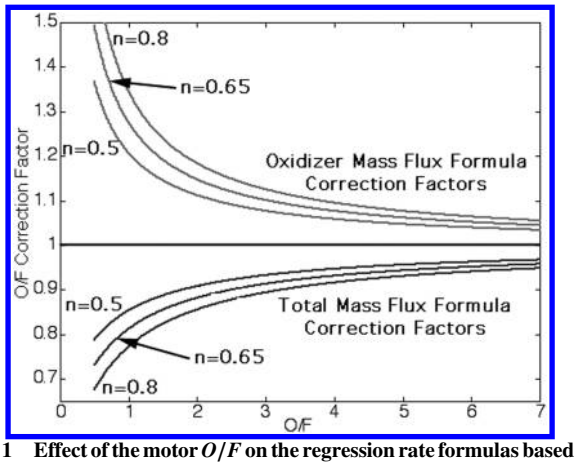

Fig. 1 Effect of the motor O/F on the regression rate formulas based on the oxidizer mass flux and total mass flux.

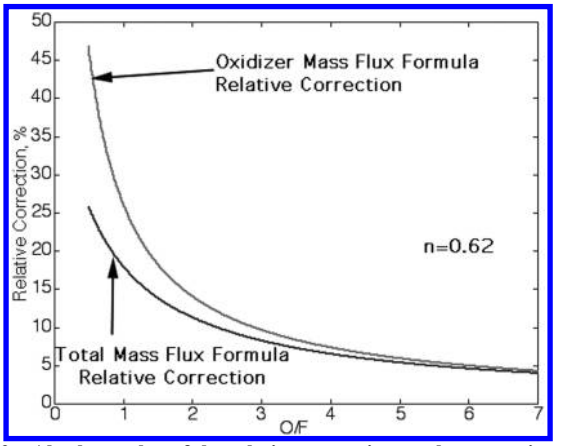

Fig. 2 Absolute value of the relative correction on the regression rate formulas based on the oxidizer mass flux and total mass flux as a function of motor O/F.

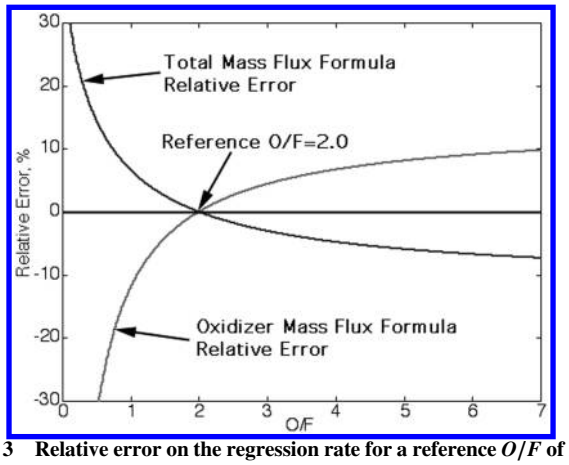

Fig. 3 Relative error on the regression rate for a reference O/F of 2.0.

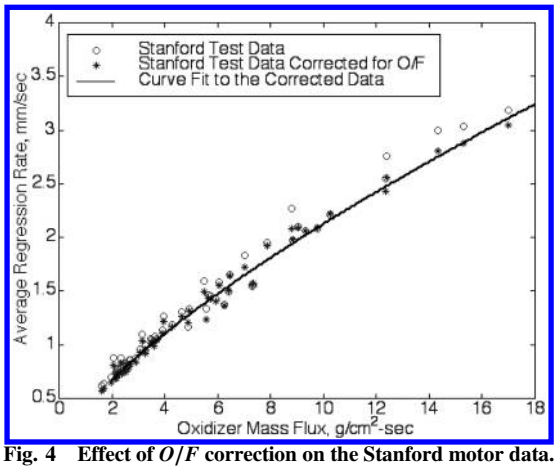

Fig. 4 Effect of O/F correction on the Stanford motor data.

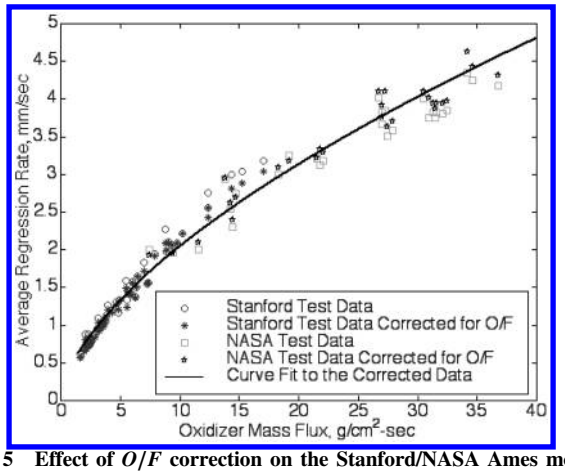

Fig. 5 Effect of O/F correction on the Stanford/NASA Ames motor data.

for O/F larger than 3–4, the deviation between the two methods becomes negligible.

Figure 3 shows the errors in percent relative to a reference O/F of 2.0. Based on this figure, the correction for a system operating at an O/F of 1.0 produces an error of more than 10% when the uncorrected oxidizer mass flux expression is used and more than 6% when the total flux approach is implemented. The errors for a motor operating at an O/F of 3.0 (i.e., equidistant from the reference O/F of 2.0 in the fuel lean direction) are 4.2 and 3% for the oxidizer and total mass flux methods, respectively. We also like to note that, if the O/F correction formulas are used, the selection of the oxidizer mass flux or the total flux based scaling formulas is completely arbitrary.

The use of formulas for data reduction from the motor tests or for ballistic calculations is an iterative process. In the case of motor testing, the O/F for each test is directly measured but the regression rate flux exponent n is not known a priori. The correct n must be obtained following an iterative process. For the ballistic calculations, at each instance of the operation (the flux exponent is known) the motor O/F is not available, because it requires the knowledge of regression rate which itself is a function of O/F. Thus, the regression rate must be obtained following an iterative process. For systems operating at high O/F ratios, such as H_2O_2 motors, the effect of space averaging can be ignored.

The effectiveness of the space-averaging technique has been examined using the extensive data set from the paraffin-based fuel SP-1a/GOX motor tests conducted at Stanford University and NASA Ames Research Center [4,5]. We first concentrate on the Stanford test data collected using a 3 in. o.d. lab scale motor. This set is ideal for verifying the applicability of the O/F correction because there are 60 tests in the matrix with a wide variation in O/F ranging from 1.0 to 2.5. For the moment, the length exponent is assumed to be zero for this particular propellant combination. The best curve fit expression estimated for the Stanford data is

$$\bar{\dot{r}} = 0.077\bar{G}_o^{0.72} \tag{27}$$

Here, the units are millimeters per second for the regression rate and kilograms per meters squared (per second) for the oxidizer mass flux. This curve fit formula is determined for the transformed regression rate data set evaluated at an arbitrarily selected motor O/F of 2.0. This transformation operation can be written simply as

$$\bar{\dot{r}} = \bar{\dot{r}}_{\text{raw}} \frac{f_o(2)}{f_o(O/F)} \tag{28}$$

Note that this process needs to be repeated until the oxidizer mass flux exponent obtained as a curve fit to the modified regression rate data converges. It has been observed that this iteration procedure is fairly well behaved and the convergence is achieved in a few steps. Also note that $\bar{\dot{r}}$ value estimated using Eq. (28) is the regression rate expected for a motor operating at an O/F of 2.0.

In Fig. 4, the raw and modified regression rate data are plotted as a function of the oxidizer mass flux. A plot of the curve fit expression is also included in the figure. Note that the scatter in the modified data is reduced compared with the scatter in the raw data. In fact, the norm of the residuals is reduced from a value of 0.4695 for the raw data to 0.3941 for the modified set. Note that the error norms are estimated based on the best fits for each data set.

Similar arguments can be made for the combined data from Stanford and NASA motor tests. The best-fit regression rate obtained for the combined set is

$$\bar{\dot{r}} = 0.117\bar{G}_o^{0.62} \tag{29}$$

Here, the units are millimeters per second for the regression rate and kilograms per meters squared (per second) for the oxidizer mass flux. The reduction in the data scatter is shown in Fig. 5 for the combined Stanford NASA data set. The error norm has also improved from 0.334 to 0.293 after the application of the O/F correction on the raw data.

The O/F correction has also been applied to the Joint Government/Industry Research and Development (JIRAD) motors [1]. Unlike the paraffin data, no reduction in the scatter has been observed. We believe that the limited number tests (i.e., nine burn rate tests), the relatively high O/F ratios, and the narrow range of O/F in the test matrix are potential reasons for the inconclusiveness of the space correction procedure outlined in this paper.

IV. Time Averaging

In this section, we concentrate on the time-averaging issues one encounters in the testing and design of hybrid rocket systems. For simplicity, the effects of the space averaging will be ignored and, for the purposes of this section, the fuel will be assumed to be burning uniformly along the length of the grain.

The estimation of a well-defined and unique time-averaged regression rate from motor data is straightforward [i.e., see Eq. (38)]. However, due to the nonlinear nature of the flux formula, the calculation of the oxidizer mass flux is not unique. The following are the three types of time-averaging methods that are commonly used in the hybrid field:

1) Based on port diameter, the arithmetic average of the initial and the final port diameters is used in the calculation.

$$\bar{G}_{\text{oD}} = \frac{16\dot{m}_o}{\pi(D_i + D_f)^2} \tag{30}$$

Equation (30) takes the following form when it is written in terms of the final to initial port diameter ratio, $R \equiv D_f/D_i$.

$$\bar{G}_{\text{oD}} = \frac{16}{\pi}\frac{\dot{m}_o}{D_i^2}\frac{1}{(R+1)^2} \tag{31}$$

2) Based on port area, one uses the arithmetic average of the initial and final port areas.

$$\bar{G}_{\text{oA}} = \frac{2\dot{m}_o}{A_{\text{port}i} + A_{\text{port}f}} \tag{32}$$

This can be written in terms of R as

$$\bar{G}_{\text{oA}} = \frac{8}{\pi}\frac{\dot{m}_o}{D_i^2}\frac{1}{R^2+1} \tag{33}$$

3) Based on mass flux, one uses the average oxidizer mass flux at ignition and at thrust termination.

$$\bar{G}_{\text{oF}} = 0.5\left(\frac{\dot{m}_o}{A_{\text{port}i}} + \frac{\dot{m}_o}{A_{\text{port}f}}\right) \tag{34}$$

This can also be expressed in terms of R as

$$\bar{G}_{\text{oF}} = \frac{2}{\pi}\frac{\dot{m}_o}{D_i^2}\frac{R^2+1}{R^2} \tag{35}$$

Please note that the list of averaging techniques given in the preceding paragraphs is not complete. These are just the methods that are commonly used in the field. It can be argued that all of these averaging techniques result in different mass fluxes for the same measured regression rates. Consequently, different regression rate laws can be generated for each method for the same set of test data.

Here, we will develop estimates for the error introduced by using these approximate expressions for the oxidizer mass flux. The comparison will be based on the exact formula which can be derived from the time integration of the port diameter. For a single circular port system, the variation of the port diameter is governed by

$$\frac{dD}{dt} = 2\dot{r} = 2aG_o^n = C_D\frac{\dot{m}_o^n}{D^{2n}} \tag{36a}$$

where

$$C_D = \frac{a2^{2n+1}}{\pi^n} \tag{36b}$$

For constant oxidizer mass flow rate, this equation can be integrated by separation of variables to obtain the following relation between the final and initial diameters.

$$D_f^{2n+1} = D_i^{2n+1} + (2n+1)C_D\dot{m}_o^n t_b \tag{37}$$

The exact oxidizer mass flux associated with the average regression rate

$$\bar{\dot{r}} \cong \frac{D_{pf} - D_{pi}}{2t_b} \tag{38}$$

can be derived form the regression rate law as

$$\bar{G}_{\text{oE}} = \left[\frac{D_f - D_i}{2at_b}\right]^{1/n} \tag{39}$$

The burn time can be eliminated from Eqs. (37) and (39) to obtain the following expression for the exact mass flux.

$$\bar{G}_{\text{oE}} = \kappa\left[\frac{D_f - D_i}{D_f^{2n+1} - D_i^{2n+1}}\right]^{1/n}\dot{m}_o \tag{40}$$

where

$$\kappa = \frac{4}{\pi}(2n+1)^{1/n}$$

In terms of the diameter ratio, $R = D_f/D_i$, this formula can be written as

$$\bar{G}_{\text{oE}} = \kappa\frac{\dot{m}_o}{D_i^2}\left[\frac{R-1}{R^{2n+1}-1}\right]^{1/n} \tag{41}$$

Arguably, all of the oxidizer mass flux estimates based on Eqs. (31), (33), and (35) are inaccurate, as they produce mass fluxes different from the exact formula given by Eq. (41). Figure 6 demonstrates this fact in the regression rate/oxidizer mass flux plane. The exact variation of the regression rate over the course of the burn for a propellant following the instantaneous regression rate law is plotted in the figure. The average regression rate for this particular case is approximately 3.9 mm/s corresponding to an exact oxidizer mass flux of approximately 29 g/cm$^2 \cdot$ s. As also shown in the figure, the fluxes estimated by three separate methods have the following ranking of error in increasing order: diameter averaging, area averaging, and flux averaging. The error for the diameter averaging, for this particular example, is negligible, whereas the errors for the area averaging and especially flux averaging are unacceptably high.

The following formulas give the ratio of the predicted oxidizer mass flux for each averaging technique to the exact mass flux as a function of the diameter ratio and the oxidizer mass flux exponent.

$$\text{Error}_D \equiv \frac{\bar{G}_{\text{oD}}}{\bar{G}_{\text{oE}}} = \frac{16}{\pi\kappa}\left[\frac{R^{2n+1}-1}{(R+1)^{2n}(R-1)}\right]^{1/n} \tag{42}$$

$$\text{Error}_A \equiv \frac{\bar{G}_{\text{oA}}}{\bar{G}_{\text{oE}}} = \frac{8}{\pi\kappa}\left[\frac{R^{2n+1}-1}{(R^2+1)^{n}(R-1)}\right]^{1/n} \tag{43}$$

$$\text{Error}_F \equiv \frac{\bar{G}_{\text{oF}}}{\bar{G}_{\text{oE}}} = \frac{2}{\pi\kappa}\left[\frac{(R^2+1)^n(R^{2n+1}-1)}{(R-1)R^{2n}}\right]^{1/n} \tag{44}$$

Note that these expressions present the systematic error associated with each technique in a ratio format. An important observation is

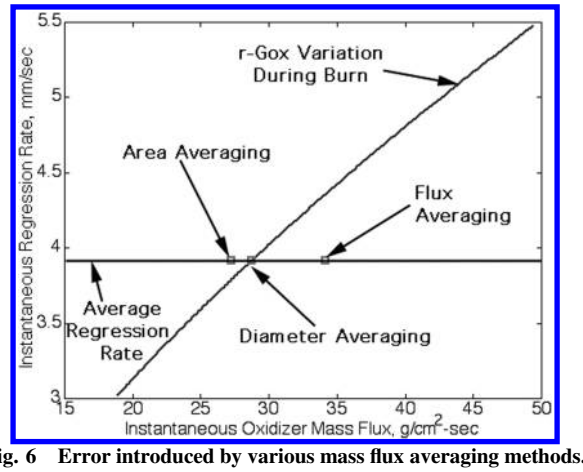

Fig. 6 Error introduced by various mass flux averaging methods.

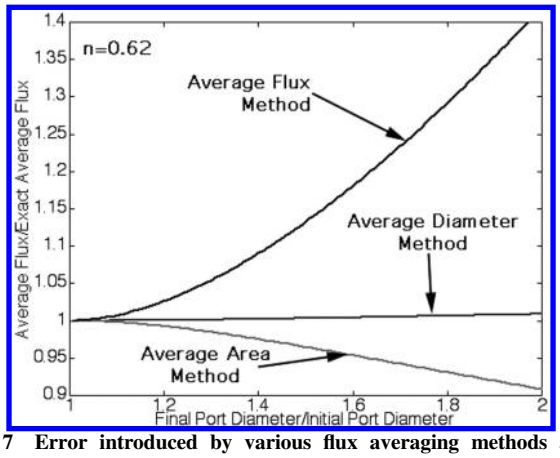

Fig. 7 Error introduced by various flux averaging methods as a function of the port diameter ratio.

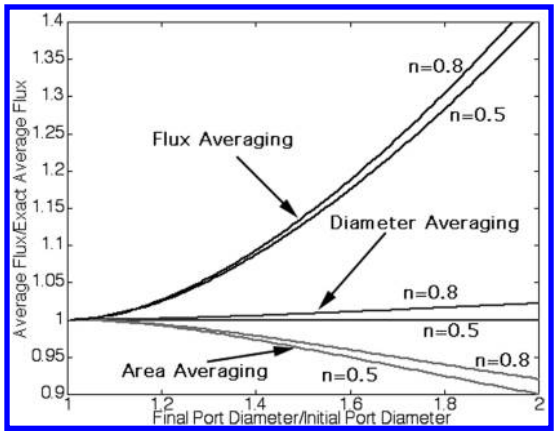

Fig. 8 Effect of the flux exponent n on the error introduced by various flux averaging methods.

that if the oxidizer mass flux exponent is 0.5, Error_D becomes 1.0, indicating that for $n = 0.5$, the diameter averaging technique is exact.

In Fig. 7, the percent errors produced by the Eqs. (42–44) are plotted against the diameter ratio for an oxidizer mass flux exponent of 0.62. It is clear from the figure that by far the most accurate technique to estimate the oxidizer mass flux is based on the port diameter averaging. Note that the area averaging method significantly underestimates the flux, whereas the flux averaging grossly overestimates. Figure 8 demonstrates the effect of the oxidizer mass flux exponent on the systematic error for all of the three techniques discussed in this section. The influence of n on the error is different for each technique. For flux averaging and diameter averaging, error increases with growing n (at least in the range $0.5 < n < 0.8$), whereas the opposite trend holds for the area averaging.

V. Estimation of Combined Error

It is critical to evaluate and control the error in estimating the regression rate law from a set of motor tests. A comprehensive error model is essential to understand the accuracy of the predicted regression rate formula and also to minimize the total error by carefully selecting the test conditions. In reality, the systematic error introduced by using a particular time-averaging method should be coupled with the random error associated with the measurements to estimate the total error on the regression rate and the oxidizer mass flux. The scaling of the systematic error has been discussed in detail in the previous section. In the following paragraphs we will develop formulas to predict the random measurement errors and couple these with the systematic ones to calculate the combined error associated with each motor test.

The time-averaged regression rate for a given test can be estimated using Eq. (38). In practice, the final port diameter that appears in the regression rate equation can be most accurately estimated based on the consumed fuel mass measurement using the following equation.

$$D_f = \left[D_i^2 + \frac{4\Delta M_f}{\pi \rho_f L} \right]^{1/2} \tag{45}$$

With the use of Eq. (45), the relative random error in the final diameter E_{df} can be written in terms of the relative measurement errors in fuel grain mass loss $E_{\Delta M}$, initial port diameter E_{di}, fuel density E_ρ, and grain length E_L.

$$E_{\text{df}} = \left[\left(\frac{E_{\text{di}}}{R} \right)^2 + 0.5 \left(1 - \frac{1}{R^2} \right)^2 (E_{\Delta M}^2 + E_\rho^2 + E_L^2) \right]^{1/2} \tag{46}$$

Similarly, the relative random error in the regression rate estimation E_r can be written in terms of the relative errors in the final port diameter E_{df}, initial port diameter E_{di}, and the burn time E_t.

$$E_r = \left[\left(\frac{R}{R-1} E_{\text{df}} \right)^2 + \left(\frac{1}{R-1} E_{\text{di}} \right)^2 + E_t^2 \right]^{1/2} \tag{47}$$

By using Eqs. (46) and (47), the random error in regression rate can be estimated based on the measurement errors in initial port diameter, fuel weight reduction, fuel density, grain length, and burn time. Note that the relative error in the regression rate decreases with increasing diameter ratio, $R = D_f/D_i$, or web thickness burned. The effects of the ignition and shutdown processes on the regression rate error is included in the error associated with the burn time. For systems with excessive ignition or thrust termination lag times, enhanced corrections must be developed as discussed in [4].

For a typical test with the following parameters and measurement errors, the relative and absolute errors in the regression rate can be estimated to be 0.051 and 0.159 mm/s, respectively.

$$\bar{\dot{r}} = 3.130 \text{ mm/s}, \quad n = 0.62, \quad t_b = 8.00 \text{ s}$$
$$D_i = 10.16 \text{ cm}, \quad D_f = 15.66 \text{ cm} \quad E_{\Delta M} = 0.010$$
$$E_\rho = 0.011, \quad E_L = 0.002, \quad E_{\text{di}} = 0.008, \quad E_t = 0.013$$

Similarly, Eq. (30) can be used to determine the relative error in the oxidizer mass flux E_{Go} in the case of diameter averaging.

$$E_{\text{Go}} = \left[\left(\frac{2R}{R-1} E_{\text{df}} \right)^2 + \left(\frac{2}{R-1} E_{\text{di}} \right)^2 + E_{\text{mox}}^2 \right]^{1/2} \tag{48}$$

Note that similar expressions for the other averaging methods can be derived.

The relative error in the oxidizer mass flow rate depends on the details of the oxidizer feed system used in the tests. For the particular case of a gaseous oxidizer feed system with a choked orifice, the flow rate is controlled by the following equation.

$$\dot{m}_o = \frac{P_f A_{\text{or}} C_d}{c_o^*} \tag{49}$$

As a first guess, the discharge coefficient Cd for the thick, square-edge orifice can be taken as 0.84 [4].

Based on the orifice equation, the relative error in the oxidizer mass flow rate E_{mo} can be calculated in terms of the relative errors in the average feed pressure E_{Pf}, orifice diameter E_{do}, orifice discharge coefficient E_{Cd}, and tank temperature E_{To}.

$$E_{\text{mo}} = \left[E_{\text{Pf}}^2 + (2E_{\text{do}})^2 + E_{\text{Cd}}^2 + (E_{\text{To}}/2)^2 \right]^{1/2} \tag{50}$$

For a typical test characterized by the following conditions, the relative and absolute random errors associated with the oxidizer mass flux estimation can be calculated to be 0.037 and 0.730 $\text{g/cm}^2 \cdot \text{s}$, respectively.

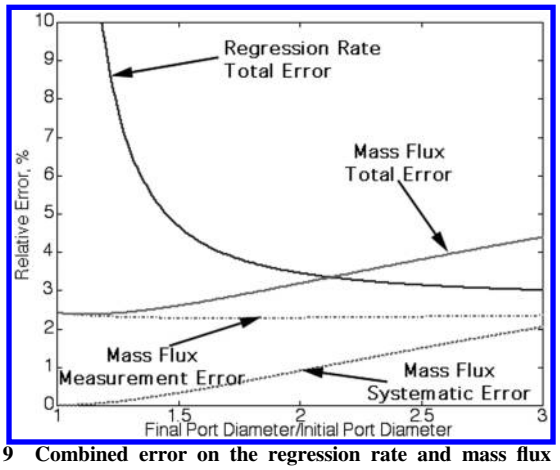

Fig. 9 Combined error on the regression rate and mass flux as a function of diameter ratio.

$$\bar{G}_o = 20.0\ \text{g/cm}^2 \cdot \text{s}, \qquad E_{\text{Pf}} = 0.020, \qquad E_{\text{do}} = 0.001$$
$$E_{\text{Cd}} = 0.024, \qquad E_{\text{To}} = 0.010$$

The total error for the regression rate and the oxidizer mass flux is a combination of the systematic error given by Eqs. (42–44) for the oxidizer mass flux and the random measurement errors given by Eq. (47) (for the regression rate) and Eq. (48) (for the oxidizer mass flux). Note that the systematic error on the regression rate estimation is zero.

A careful examination reveals that both the systematic and the random error expressions are functions of the diameter ratio. For the test conditions and measurement errors outlined in the previous paragraphs, the combined errors and its components are plotted in Fig. 9. As indicated by the figure, the systematic error in the oxidizer mass flux calculation (based on average diameter) increases with increasing R, whereas the random error is almost constant. For the regression rate, the systematic error is zero by definition and the random error decreases rapidly with increasing diameter ratio. The combined error for the regression rate decreases monotonously with R, asymptoting to zero at infinite diameter ratio. Note that the total errors for the regression rate and the oxidizer mass flux follow opposite trends with increasing burn time. This indicates that the test burn times need to be selected to yield an intermediate R value to obtain the most accurate burn rate expression. For the particular example that we have considered in this paper, this optimal diameter ratio is around 2.0.

VI. Combined Space–Time Averaging

In the previous sections, the space and time averaging methods for the regression rate expression has been developed separately. In reality, the spatial and temporal variation of the port hydraulic diameter are coupled together and the space and time averaging processes must be treated simultaneously. In this section, we will address the space–time coupled dynamics of the hybrid rocket fuel port. For the sake of simplicity, we will limit our analysis to the case of a single circular port, however, the following arguments can easily be extended to a wide range of port geometries.

Based on the definition of regression rate, $2\dot{r} \equiv \partial D/\partial t$, the variation of the port diameter at an axial position x and time t can be written as

$$\frac{\partial D}{\partial t} = C_D \frac{\dot{m}^n x^m}{D^{2n}} \tag{51}$$

where parameter C_D is defined by Eq. (36b).

Similarly, under the quasi-steady assumption, the mass flow balance in the port requires that

$$\frac{\partial \dot{m}}{\partial x} = C_m \frac{\dot{m}^n x^m}{D^{2n-1}} \tag{52a}$$

where the constant is defined as

$$C_m = a\rho_f 2^{2n} \pi^{1-n} \tag{52b}$$

Equations (51) and (52a) constitute two nonlinear first-order partial differential equations (PDEs) which could be solved to determine the space–time variation of the two key variables, $\dot{m}(x,t)$ and $D(x,t)$. The initial condition $[D(x,t=0) = D_i(x)]$ and boundary condition $[\dot{m}(x=0,t) = \dot{m}_o(t)]$ needed to solve the problem are the oxidizer flow rate time history and the initial port diameter distribution, respectively.

A. Numerical Solutions

Presently, no closed form solutions (other than for $n = 0.5$) could be obtained for the set of nonlinear PDEs governing the dynamics of the fuel port diameter. However, we recommend the following method for numerical integration.

Rearrangement of Eq. (52a) results in the separation of the mass flow rate term as

$$\frac{\partial \dot{m}^{1-n}}{\partial x} = C_m \frac{x^m}{D^{2n-1}} \tag{53}$$

The integration on the x variable results in

$$\dot{m} = \left[\dot{m}_o^{1-n} + (1-n) C_m \int_0^x \frac{\tilde{x}^m}{D^{2n-1}}\, \mathrm{d}\tilde{x} \right]^{1/1-n} \tag{54}$$

Equation (54) can be substituted into Eq. (51) to obtain the following integro-differential equation

$$\frac{\partial D}{\partial t} = C_D \frac{x^m}{D^{2n}} \left[\dot{m}_o^{1-n} + (1-n) C_m \int_0^x \frac{\tilde{x}^m}{D^{2n-1}}\, \mathrm{d}\tilde{x} \right]^{n/1-n} \tag{55}$$

Numerical solutions for Eq. (55) have been obtained by implementing an RK4 scheme (the classical fourth-order Runge–Kutta

Table 1 Summary of motor test data used to evaluate the length exponent for the paraffin/GOX system

Test	4L-04	4L-05	4L-08	4P-01
Oxidizer mass flow rate, kg/s	4.44	4.43	4.42	4.43
Burn time, s	8.30	8.25	8.15	8.40
Average O/F	2.66	2.72	2.64	2.69
Initial port diameter, cm	8.93	10.01	10.30	11.38
Grain length, m	1.149	1.149	1.148	1.148
Final port diameter (fore end), cm	15.53	15.88	16.17	16.67
Final port diameter (aft end), cm	16.23	16.63	16.64	17.54
Axial change in the port diameter, %	4.34	4.54	2.84	4.99
Flux exponent, n	0.62	0.62	0.62	0.62
Length exponent, m	−0.018	−0.009	−0.033	0.000
Regression rate coefficient, a[a]	$9.36 \cdot 10^{-2}$	$9.24 \cdot 10^{-2}$	$9.10 \cdot 10^{-2}$	$9.36 \cdot 10^{-2}$

[a]Note that the units of the regression rate coefficient are based on millimeters per second for the regression rate, meters for the length, and kilograms per meters squared (per second) for the mass flux.

method) for time marching and the trapezoidal method for the spatial integration. This method has been used to produce accurate predictions for the port diameter dynamics using very limited CPU time. In fact, the runs for most cases took less than 20 s on a desktop PC.

B. Discussion of Results

The space–time coupled dynamic method has been applied to some of the paraffin/GOX motor tests conducted at the Hybrid Combustion Facility of NASA Ames Research Center [4]. Reliable posttest port diameter measurements were taken at the fore and aft ends of the fuel grain for four of the motor tests conducted in the program. The summary of the relevant data for these tests is given in Table 1. For all cases, an oxidizer mass flux exponent of 0.62 has been used in the calculations. The length exponent and the regression rate coefficient has been calculated for each test by matching the predicted fore and aft port diameters to the measured values. All tests, each conducted at different operating conditions, resulted in length exponents in the narrow range of −0.033 to 0.000 with an average value of −0.015. Note that the variation in the estimated m values is well within the measurement error for the diameters used in the calculations. Similarly, the estimated regression rate coefficients varied in the narrow range of 0.0910–0.0936 and averaged at a value of 0.0927. Note that the units of the coefficient a are based on millimeter per second for the regression rate, meters for length, and kilograms per meters squared (per second) for the oxidizer mass flux.

Figure 10 shows the fuel port radius contours as a function of time calculated by the numerical integration procedure discussed in the previous paragraphs using the values of $n = 0.62$, $m = -0.015$, and $a = 0.0927$. The oxidizer mass flow rate is assumed to be constant in time with a value of 4.5 kg/s and the fuel density is taken as 920 kg/m^3. For the simulated case, the initial port diameter is 0.106 m and the fuel grain length is 1.144 m. The figure shows that the port diameter for all times (other than $t = 0$) has a minimum at a point close to the fore end and it increases monotonically from its minimum value with increasing axial distance. The part of the curves that is very close to the leading edge are not shown because in this region the regression rate expression, which is based on boundary layer arguments, ceases to be valid (in fact, it incorrectly predicts infinite regression rate at $x = 0$). This is a narrow region for most hybrid applications and will be ignored in this paper. Also note that the surface contours get closer as the time progresses, indicating a lower regression rate due to reduced mass flux.

The distribution of the residual fuel as a function of time has been plotted in Fig. 11 for various burn times. Note that each burn time corresponds to a different motor with the grain outside diameter (or motor case inside diameter) matched to the port diameter at the exit plane. It is important to understand that the curves are not plotted to scale and the y axis is amplified significantly compared to the x axis. As indicated by the figure, initially, the residual fuel increases sharply with time. As the time progresses, the increase in the residual web slows down due to the self-correcting nature of the hybrid

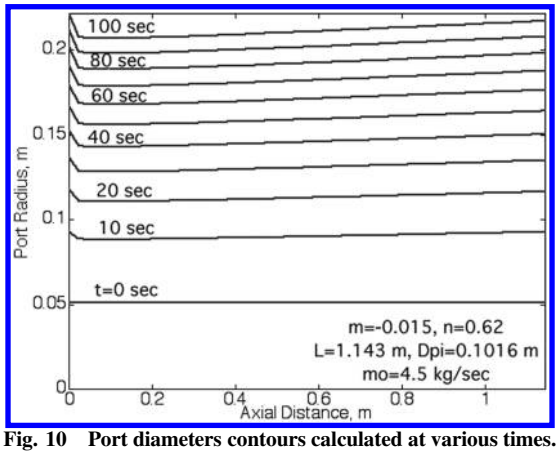

Fig. 10 Port diameters contours calculated at various times.

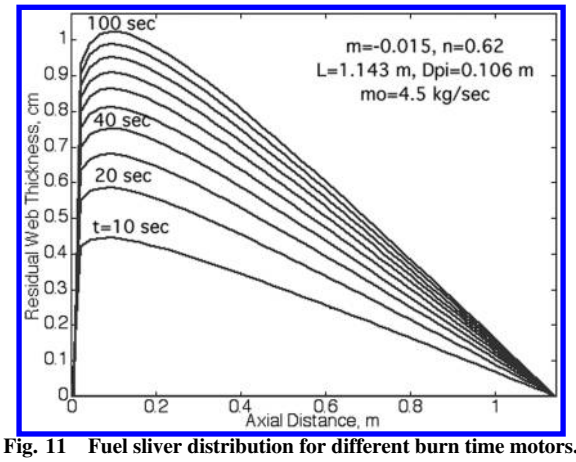

Fig. 11 Fuel sliver distribution for different burn time motors.

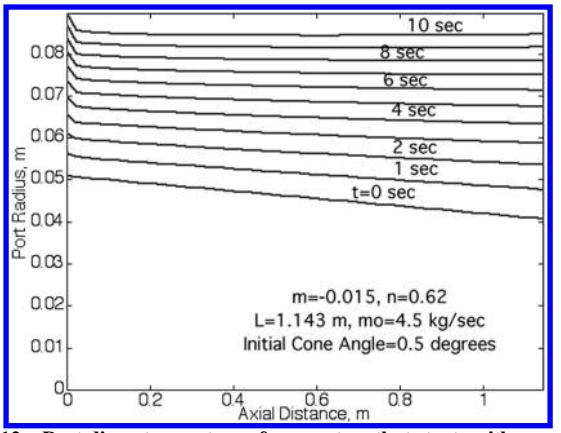

Fig. 12 Port diameter contours for a system that starts with a conical geometry.

regression rate dynamics, namely, as the port opens up more in one particular area, the regression rate drops because of the decrease in the local mass flux.

A regression rate law with a length exponent close to zero (as in the case of paraffin/GOX) is a highly desirable virtue, because it makes the regression rate insensitive to the overall scale of the propulsion system. For such cases, the regression rate law derived from small scale motor tests can be used, with reasonable confidence, to conduct the ballistic design of a full-scale hybrid system. However, we must state that other important design parameters such as the combustion efficiency and stability would still be scale dependent. Therefore, even for $m = 0$, at each scale, significant motor testing effort would still be required.

The shortcoming of the weak negative length dependency, for which the mass flux is the only practical regression rate driver, is the increased nonuniformity in the regression rate of the hybrid fuel. This can be observed in Figs. 10 and 11 for the example system. Note that even for the worst case, the average sliver thickness is relatively small, resulting in a much smaller residual fuel mass fraction compared with a multiport system. This minor shortcoming can be eliminated for a single circular port hybrid by slightly coning the initial port geometry. As shown in Fig. 12, a 0.5 deg coning reduces the sliver dramatically for a system with $t_b = 10$ s.

C. Exact Solution for $n = 0.5$

An exact solution for Eqs. (51) and (52a) can be obtained for the special case corresponding to a flux exponent of 0.5. In this particular situation, the mass flow rate equation looses its explicit dependency on the port diameter and can be written in the following form.

$$\frac{\partial \dot{m}^{0.5}}{\partial x} = 0.5 C_m x^m \tag{56}$$

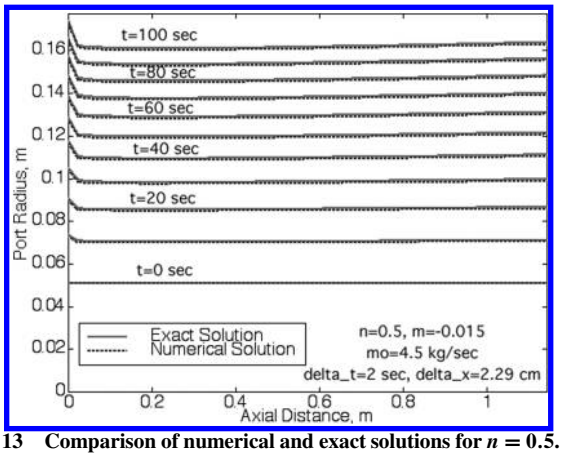

Fig. 13 Comparison of numerical and exact solutions for $n = 0.5$. The spatial step is 2.29 cm.

Integration in the x variable yields the solution for the mass flow rate.

$$\dot{m}(x,t) = \left(\sqrt{\dot{m}_o(t)} + \frac{0.5C_m}{m+1}x^{m+1}\right)^2 \tag{57}$$

Substitution of Eq. (57) into Eq. (51) and time integration gives the exact solution for the port diameter as a function of time and distance.

$$D(x,t) = \left(D_i^2(x) + 2C_D x^m \int_o^t \sqrt{\dot{m}_o(\tilde{t})}\,\mathrm{d}\tilde{t} + \frac{C_D C_m}{m+1}x^{2m+1}t\right)^{1/2} \tag{58}$$

For the special case of constant oxidizer mass flow rate, Eq. (58) becomes

$$D(x,t) = \left[D_i^2(x) + C_D x^m t\left(2\sqrt{\dot{m}_o} + \frac{C_m}{m+1}x^{2m+1}\right)\right]^{1/2} \tag{59}$$

Finally, for $m = 0$ the port diameter takes the simple form

$$D(x,t) = \left[D_i^2(x) + C_D t(2\sqrt{\dot{m}_o} + C_m x)\right]^{1/2} \tag{60}$$

The exact solution (for the case of constant oxidizer mass flow rate) given by Eq. (59) has been used to check the accuracy of the numerical solutions described in the previous section. Figure 13 shows the port radius contours at various times for the exact solution and also for the numerical simulation which was conducted under identical conditions. As indicated by the figure, even for the relatively coarse time step of 2 s used in the simulations, the agreement between the two solutions is perfect for all times. Moreover, by cutting the time step by half (down to 1 s), we have managed to further reduce the error to a value which can be taken to be zero for all practical purposes. It is expected that the numerical solutions would also be highly accurate at other values of the flux exponent for which no exact solutions exist.

D. Global Mass Balance

We will close this section by deriving a useful global relation for the mass balance. Equations (51) and (52a) can be combined to eliminate the common terms that appear on the right-hand side of both equations.

$$\frac{\partial \dot{m}}{\partial x} = \frac{C_m}{2C_D}\frac{\partial D^2}{\partial t} \tag{61}$$

Using the definition of the coefficients, Eq. (61) can be reduced to

$$\frac{\partial \dot{m}}{\partial x} = \frac{\partial(\rho_f A_{\text{port}})}{\partial t} \tag{62}$$

Integration in the x variable results in

$$\dot{m} - \dot{m}_o = \frac{\partial(\rho_f V_{\text{port}x})}{\partial t} \tag{63}$$

Equation (63) states the obvious requirement that the fuel mass addition from the leading edge to an arbitrary point x must be equal to the increase in the volume of the port in the same region times the density of the solid fuel. The global mass balance, given by Eq. (63), can be used to check the accuracy of the numerical solutions.

VII. Conclusions

The following conclusions can be drawn from this study.

1) Nondimensional formulas for space-averaging have been derived for the separate cases of oxidizer and total mass flux dependent regression rate laws. The correction term which only depends on the motor O/F is determined to be more pronounced for systems operating under fuel rich conditions. The case of oxidizer mass flux requires a slightly higher correction compared to the total mass flux formula. The O/F correction reduced the scatter in data for the paraffin/GOX motors tested at Stanford and NASA Ames facilities. The effect of correction on the JIRAD data (HTPB/GOX propellant system) was not conclusive, possibly due to the narrow range of operational parameters for this particular data set. At this point, we would like to emphasize that none of the assumptions introduced in the derivations are related to the type or properties of the selected fuel. Thus, we fully expect that the results are universal for any inert hybrid fuel system.

2) Various time-averaging techniques for the mass flux have been evaluated based on their relative accuracies compared to the exact expression. It has been determined that the diameter-based averaging method is by far the most accurate technique. It is important that each separate method selected to reduce the oxidizer mass flux data results in a significantly different regression rate law even for the same set of motor data. Therefore, the method used in the analysis must be explicitly stated in reporting the regression rate/mass flux data.

3) The systematic and random measurement errors for the regression rate and the oxidizer mass flux have been investigated. Several equations to predict both kinds of error have been derived. It has been determined that the most important variable that affects the combined error is the final to initial port diameter of the test articles. There exists an optimal value for the diameter ratio that minimizes the combined error in the regression rate and the oxidizer mass flux. For the example considered in this paper, the optimal ratio is determined to be around 2.0.

4) Finally, the partial differential equations that govern the space–time coupled dynamics of the port geometry in the simple case of a circular port have been derived. An exact solution for the special case of $n = 0.5$ has been developed. For all other mass flux exponents, an efficient and accurate numerical solution method has been suggested. The method has been applied to the case of paraffin-based fuels burned with GOX. The results indicated a very weak length dependency in the regression rate law. This observation is consistent with the experimental results [4] which showed no measurable change in the regression rate as the motor scale has been increased by a factor of 3.0.

Acknowledgment

This work was supported by Stanford University Department of Aeronautics and Astronautics gift funds.

References

[1] Boardman, T. A., Carpenter, R. L., Goldberg, B. E., and Shaeffer, C. W., "Development and Testing of 11- and 24 inch Hybrid Motors Under the Joint Government/Industry IR&D Program," *AIAA/SAE/ASME/ASEE 29th Joint Propulsion Conference and Exhibit, Monterey, CA*, AIAA Paper No. 93-2552, June 1993.

[2] Marxman G. A., Wooldridge, C. E., and Muzzy, R. J., "*Fundamentals of Hybrid Boundary Layer Combustion*," Vol. 15, Progress in Astronautics and Aeronautics, AIAA, New York, 1964, pp. 485–522.

[3] Chiaverini, M. J., Serin, N., Johnson, D., Lu, Y. C., Kuo, K. K., and Risha, G. A., "Regression Rate Behavior of Hybrid Rocket Solid

Fuels," *Journal of Propulsion and Power*, Vol. 16, No. 1, Jan.–Feb. 2000, pp. 125–132.
[4] Karabeyoglu, M. A., Zilliac, G., Cantwell, B. J., DeZilwa, S., and Castellucci, P., "Scale-Up Tests of High Regression Rate Paraffin-Based Hybrid Rocket Fuels," *Journal of Propulsion and Power*, Vol. 20, No. 6, 2004, pp. 1037–1045.
[5] Karabeyoglu, M. A., Cantwell, B. J., and Altman, D., "Development and Testing of Paraffin-Based Hybrid Rocket Fuels," *37th AIAA/ASME/SAE/ASEE Joint Propulsion Conference and Exhibit, Salt Lake City, Utah*, AIAA Paper 2001-4503, July 2001.

S. Son
Associate Editor

This article has been cited by:

1. Mehmet Kahraman, Kaan Gegeoglu, Ibrahim Ozkol, Arif M. Karabeyoglu. Novel Hybrid Rocket Internal Ballistic Configuration with Coaxially Located Tube Injector . [Citation] [PDF] [PDF Plus]
2. Hakki Karakas, Ozan Kara, Ibrahim Ozkol, Arif M. Karabeyoglu. Performance Enhancing Additives for Hybrid Rockets . [Citation] [PDF] [PDF Plus]
3. Connor C. McDougall, Colin Hill, Cynthia Heinrichs, Craig T. Johansen. Spectroscopic Techniques for Measuring Regression Rates of Liquefying Hybrid Rocket Fuels . [Citation] [PDF] [PDF Plus]
4. Kaan Gegeoglu, Mehmet Kahraman, Caglar Ucler, Arif Karabeyoglu. Assessment of Using Electric Pumps on Hybrid Rockets . [Citation] [PDF] [PDF Plus]
5. Daniele Bianchi, Giuseppe Leccese, Francesco Nasuti, Marcello Onofri, Carmine Carmicino. 2019. Modeling of High Density Polyethylene Regression Rate in the Simulation of Hybrid Rocket Flowfields. *Aerospace* **6**:8, 88. [Crossref]
6. G.D. Di Martino, S. Mungiguerra, C. Carmicino, R. Savino. 2019. Computational fluid-dynamic modeling of the internal ballistics of paraffin-fueled hybrid rocket. *Aerospace Science and Technology* **89**, 431-444. [Crossref]
7. Suhang Chen, Yue Tang, Hongsheng Yu, Xinyan Guan, Luigi T. DeLuca, Wei Zhang, Ruiqi Shen, Yinghua Ye. 2019. Combustion enhancement of hydroxyl-terminated polybutadiene by doping multiwall carbon nanotubes. *Carbon* **144**, 472-480. [Crossref]
8. Kohei Ozawa, Koki Kitagawa, Shigeru Aso, Toru Shimada. 2019. Hybrid Rocket Firing Experiments at Various Axial–Tangential Oxidizer-Flow-Rate Ratios. *Journal of Propulsion and Power* **35**:1, 94-108. [Abstract] [Full Text] [PDF] [PDF Plus]
9. M. Kobald, C. Schmierer, U. Fischer, K. Tomilin, A. Petrarolo, M. Rehberger. The HyEnD stern hybrid sounding rocket project 25-64. [Crossref]
10. Yi Wu, Xilong Yu, Xin Lin, Sen Li, Xiaolin Wei, Chuan Zhu, Linlin Wu. 2018. Experimental investigation of fuel composition and mix-enhancer effects on the performance of paraffin-based hybrid rocket motors. *Aerospace Science and Technology* **82-83**, 620-627. [Crossref]
11. Travis Belcher, Jonathan Valenzuela, Justin Vanhoose, Ahsan R. Choudhuri, Norman D. Love. Hybrid Motor Regression Rate Using the Decomposition Products of a Green Monopropellant as the Oxidizer . [Citation] [PDF] [PDF Plus]
12. Yechiel Crispin, Naveen Sri Uddanti. Generalized Two Temperatures Approach to the Flow in the Port of a Hybrid Rocket . [Citation] [PDF] [PDF Plus]
13. Carmine Carmicino, Dario Pastrone. 2018. Novel Comprehensive Technique for Hybrid Rocket Experimental Ballistic Data Reconstruction. *Journal of Propulsion and Power* **34**:1, 133-145. [Abstract] [Full Text] [PDF] [PDF Plus]
14. Kirsty Veale, Sarp Adali, Jean Pitot, Michael Brooks. 2017. A review of the performance and structural considerations of paraffin wax hybrid rocket fuels with additives. *Acta Astronautica* **141**, 196-208. [Crossref]
15. G. D. Di Martino, C. Carmicino, R. Savino. 2017. Transient Computational Thermofluid-Dynamic Simulation of Hybrid Rocket Internal Ballistics. *Journal of Propulsion and Power* **33**:6, 1395-1409. [Abstract] [Full Text] [PDF] [PDF Plus]
16. Dongeun Lee, Changjin Lee. 2017. Fuel-Rich Combustion with Ammonium Perchlorate Addition in a Staged Hybrid Rocket Engine. *Journal of Propulsion and Power* **33**:6, 1581-1588. [Abstract] [Full Text] [PDF] [PDF Plus]
17. M. Kobald, C. Schmierer, H. K. Ciezki, S. Schlechtriem, E. Toson, L. T. De Luca. 2017. Viscosity and Regression Rate of Liquefying Hybrid Rocket Fuels. *Journal of Propulsion and Power* **33**:5, 1245-1251. [Abstract] [Full Text] [PDF] [PDF Plus]
18. Shinjae Kang, Dahae Lee, Eunkwang Lee, Sejin Kwon. Design and performance evaluation of hybrid rocket using 95 wt. % H2O2 . [Citation] [PDF] [PDF Plus]
19. Pavan Narsai, Krishna Venkataraman, Keith Javier Stober, Brian J. Cantwell. Measuring Time-Varying Fuel Regression Rates with Image Processing in a Hybrid Rocket Motor . [Citation] [PDF] [PDF Plus]
20. Carmine Carmicino, Dario Pastrone. Pressure-Measurement Based Estimation of Fuel Regression Rate in Hybrid Rockets . [Citation] [PDF] [PDF Plus]
21. Daniele Bianchi, Francesco Nasuti, Carmine Carmicino. 2016. Hybrid Rockets with Axial Injector: Port Diameter Effect on Fuel Regression Rate. *Journal of Propulsion and Power* **32**:4, 984-996. [Abstract] [Full Text] [PDF] [PDF Plus]
22. Daniele Bianchi, Francesco Nasuti, Carmine Carmicino. Numerical Analysis of Port Diameter Effect on Hybrid Rocket Fuel Regression Rate with Axial Injection . [Citation] [PDF] [PDF Plus]

23. Jungpyo Lee, Soojong Kim, Jinkon Kim, Heejang Moon. 2015. Mass Transfer Number Sensitivity on the Fuel Burning Rate in Hybrid Rockets. *Journal of Propulsion and Power* **31**:4, 1041-1050. [Abstract] [Full Text] [PDF] [PDF Plus]
24. C. Carmicino, A. Russo Sorge. 2015. Experimental Investigation into the Effect of Solid-Fuel Additives on Hybrid Rocket Performance. *Journal of Propulsion and Power* **31**:2, 699-713. [Abstract] [Full Text] [PDF] [PDF Plus]
25. Yuki Funami, Toru Shimada. Combined Analysis of Reactive Flow and Heat Transfer for Hybrid Rocket Design Engineering . [Citation] [PDF] [PDF Plus]
26. Mario Kobald, Helmut K. Ciezki, Stefan Schlechtriem, Elena Toson, Luigi De Luca. Evaluation of Paraffin-based Fuels for Hybrid Rocket Engines . [Citation] [PDF] [PDF Plus]
27. Harunori Nagata, Hisahiro Nakayama, Mikio Watanabe, Masashi Wakita, Tsuyoshi Totani. 2014. Accuracy and applicable range of a reconstruction technique for hybrid rockets. *Advances in aircraft and spacecraft science* **1**:3, 273-289. [Crossref]
28. L. Galfetti, F. Nasuti, D. Pastrone, A.M. Russo. 2014. An Italian network to improve hybrid rocket performance: Strategy and results. *Acta Astronautica* **96**, 246-260. [Crossref]
29. N. Bellomo, F. Barato, M. Faenza, M. Lazzarin, A. Bettella, D. Pavarin. 2013. Numerical and Experimental Investigation of Unidirectional Vortex Injection in Hybrid Rocket Engines. *Journal of Propulsion and Power* **29**:5, 1097-1113. [Abstract] [Full Text] [PDF] [PDF Plus]
30. Derrick Armold, J Eric Boyer, Kenneth Kuo, Jerome K. Fuller, John Desain, Thomas J. Curtiss. Test of Hybrid Rocket Fuel Grains with Swirl Patterns Fabricated Using Rapid Prototyping Technology . [Citation] [PDF] [PDF Plus]
31. Nicolas Bellomo, Martina Faenza, Francesco Barato, Alberto Bettella, Daniele Pavarin, A. Selmo. The "Vortex Reloaded" project: experimental investigation on fully tangential vortex injection in N2O - paraffin hybrid motors . [Citation] [PDF] [PDF Plus]
32. Nicolas Bellomo, Francesco Barato, Martina Faenza, Marta Lazzarin, Alberto Bettella, Daniele Pavarin. Numerical and Experimental Investigation on Vortex Injection in Hybrid Rocket Motors . [Citation] [PDF] [PDF Plus]
33. David R. Greatrix. 2009. Regression rate estimation for standard-flow hybrid rocket engines. *Aerospace Science and Technology* **13**:7, 358-363. [Crossref]